Emergence of surface states in nanoscale Cu_{2}N islands

C. D. Ruggiero, M. Badal, T. Choi, D. Gohlke, D. Stroud, and J. A. Gupta

Phys. Rev. B **83**, 245430 — Published 27 June 2011

DOI: 10.1103/PhysRevB.83.245430

Emergence of electronic states in nanoscale Cu_2N islands

C. D. Ruggiero, M. Badal, T. Choi, D. Gohlke, D. Stroud and J. A. Gupta

Department of Physics, The Ohio State University, Columbus, OH 43210, USA

Abstract

We study electronic states in nanoscale Cu_2N islands on Cu(100) using scanning tunneling microscopy and density functional theory. Tunneling spectra indicate a state at ~2V in large islands (> 20 nm^2), which shifts due to quantum confinement in smaller islands. This state is not observed for islands with fewer than ~50 atoms. In contrast, a 4V state persists down to 12 atom islands, but does not shift within experimental error. Theory suggests that these differences reflect the different effective masses of the two Cu_2N bands, as well as their coupling to a Cu surface state.

The bulk electronic band structure of solids first emerges from atomic orbitals in nanoscale clusters. The scanning tunneling microscope (STM) is a useful tool for studying the properties of nanoclusters on surfaces ranging in size from 1 to > 10^4 atoms. Tunneling spectroscopy can probe the valence orbitals of single adatoms (*1*) and the evolution of quantum confinement in atomic chains (*2*) or adatom islands (*3*), (*4*) on metal surfaces. Recently, there has been considerable interest in isolating such structures from the metal surface by an intervening few-monolayer thick insulating film (e.g. Cu_2N, NaCl, Al_2O_3, MgO) (*5*-*7*). Ultrathin insulating films are themselves a form of nanocluster; prior studies have shown that a bulk-like band gap is already established in few-layer NaCl (*8*) and MgO films (*9*). While these studies probed the influence of quantum confinement in one dimension down to the nanometer scale, the lateral sizes of such films were too large to see additional confinement effects.

Here we study the emergence of electronic states in one atomic layer thick Cu_2N films, ranging in lateral area from quasi-continuous monolayers to sub-nm^2 islands. STM measurements reveal the quantum confined blueshift of an unoccupied state with decreasing island area down to ~1.5 nm^2, corresponding to ~50 atoms. While similar quantum confined energy shifts have been observed in a variety of STM studies,(*4*) our studies extend down to smaller islands (0.5 nm^2 or 12 atoms), where the state itself is no longer observed. This trend is qualitatively reproduced in our density functional theory (DFT) calculations of the local density of states. In contrast, a higher-energy state exhibits no systematic shift with area, and persists down to the smallest islands studied. Our DFT calculations suggest that this contrasting behavior reflects the different effective masses of the two Cu_2N bands, and their proximity in energy to a Cu surface state.

Films of Cu_2N were grown by sputter deposition of atomic N onto a clean Cu(100) surface, followed by annealing at 350 °C (*10*). Mobility during annealing facilitates the self-assembly of nitrogen atoms into islands with a (2x2) periodicity (i.e. N adsorbs in every other hollow site) (*11*). We vary island size and shape by adjusting nitrogen coverage and annealing time. Low nitrogen coverage and short annealing time (~30s) leads to small, irregularly shaped islands. Increased annealing time (~2 min) makes the islands squarer, while increased nitrogen coverage forms islands up to ~5 x 5 nm^2 (*11*). These islands coalesce into quasi-continuous monolayer films with further coverage (*12*).

All measurements were made with a Createc LT-STM operating at a base temperature of 5.3 K in ultrahigh vacuum (<$1x10^{-10}$ mbar). All data shown here were collected using a cut Ir tip. We studied Cu_2N islands with three modes of tunneling spectroscopy (*10*). In ‘constant

height' mode, the STM feedback is turned off and the tunnel current is recorded as a function of voltage, $I(V)$. By adding a 5 mV_{pp} modulation at 855 Hz to the voltage, a lock-in amplifier measures the differential conductance, dI/dV. At low voltage (i.e. $< |1V|$), dI/dV is approximately proportional to the joint LDOS of tip and sample (*13*),(*14*). We also measured dI/dV while varying both voltage and tip height ('*z*-ramp' mode) or while the feedback remains active ('constant current' mode). These two modes are useful for monitoring the joint LDOS over a larger voltage range, although dI/dV is no longer simply proportional to the LDOS. Spatial maps of dI/dV at fixed voltage were obtained by recording the lock-in signal as the tip was scanned across the surface with feedback on.

Our DFT calculations were performed using the PAW method (*15*),(*16*) with a PBE parameterized GGA exchange-correlation functional (*17*), as implemented in the VASP DFT code (*18*),(*19*). We studied a monolayer film of Cu_2N, as well as 12 atom (Cu_8N_4) and 48 atom ($Cu_{32}N_{16}$) islands, all on Cu(100). We spaced islands from their periodic images by two bulk Cu lattice constants (7.2 Å). The unit cell comprised a symmetric slab of seven Cu layers, with N adsorbed on both faces to prevent unphysical multipoles, and a vacuum region of thickness equal to the Cu slab. We used unrelaxed structures, but based on experiment (*20*), we introduced a 4% vertical expansion of the outer Cu layer, with N atoms 0.4 Å above hollow sites. More intensive computations with relaxed structures, larger interisland spacing (i.e. three Cu lattice constants instead of two) or thicker Cu slabs (i.e. nine Cu layers) yielded qualitatively similar results. Numerical convergence of total energy to ~10 meV for vacuum thickness of the monolayer unit cell and *k*-points for the islands was achieved, and a 550 eV planewave cutoff energy was used.

For more accurate comparison with scanning tunneling spectroscopy, which typically probes states near the Γ point (*13*),(*14*), we calculated LDOS by using a 9x9x1 mesh of *k*-points centered on Γ, but only covering a small fraction of the surface Brillouin zone. The mesh size and areal density were maintained with successively larger unit cells for consistent numerical precision. We calculated total and projected (*s*-,*p*-,*d*-orbital) LDOS at N and Cu sites within Cu_2N. The LDOS is convolved with a Gaussian function (FWHM~0.65 eV) to produce representative spectra, given intrinsic noise in the calculations due to the finite system size (i.e. 16, 382 and 134 atoms for ML, $Cu_{32}N_{16}$ and Cu_8N_4 islands respectively), numerical precision and periodic boundary conditions (*21*).

Figure 1 compares measured dI/dV spectra (Fig. 1A) with calculated LDOS (Fig. 1B) and band structure (Fig. 1C). The data in Fig. 1A were acquired with the tip positioned over the center of a ~ 40 nm^2 island, large enough to approximate the spectra for monolayer films

(*12*). Peaks at 2.2 and 3.8 V represent unoccupied states which are the main focus of this paper. No prominent occupied states are observed at negative voltage. Rather, a gradual rise in state density starting at -1 V is followed by a sharper rise at -5.5 V. Because tunneling at large negative voltages is dominated by electrons near the sample's Fermi energy, it is difficult to probe occupied states over such a range. While the relative heights of features in Fig. 1A are sensitive to the exact tip trajectory, these characteristic features are reproduced in constant height and current modes (*10*).

The calculated band structure of monolayer Cu_2N films (Fig. 1C) is in good agreement with our STM measurements, as well as prior DFT calculations and photoelectron spectroscopy studies (*22*). Unoccupied bands are observed, with groupings near +2 eV and +4 eV at the Γ point. A dense grouping of occupied states beginning at -2 eV is attributed to the onset of Cu *d*-states (*23*). The most prominent N-derived states begin at -5 eV, similar to the onset in d*I*/d*V* in Fig. 1A.

The set of black curves for monolayer Cu_2N in Figure 1B show the total and *s*-state LDOS, projected onto an N atom, as well as the total LDOS projected onto a Cu atom. Qualitatively similar features are found in the total LDOS for N and Cu sites, although the *d*-states are more prominent for Cu sites. Experimental d*I*/d*V* spectra do not depend on whether the tip is positioned over Cu or N site, suggesting spatial averaging over several sites. The peaks at positive voltage in d*I*/d*V* correspond well to unoccupied states in the LDOS at similar energies. However, some occupied states in the total LDOS (e.g. 0, -1.5 eV) do not appear as peaks in d*I*/d*V*. We find better agreement with the *s*-state projected LDOS. This may reflect increased overlap between *s*-states and the tip's atomic orbitals (*24*), (*25*), although the atomic termination of the STM tip is not well known. We will compare the size-dependent LDOS in Fig. 1B with experiment below.

The simple particle-in-a-box model has provided a qualitative understanding of quantum confinement in surface nanostructures such as quantum corrals (*1*), adsorbate islands (*3*),(*4*) and vacancy islands (*26*). Electrons can be similarly confined to the Cu_2N islands (*27*). Figure 2A compares d*I*/d*V* spectra taken near the 2 eV state, with the tip positioned over the center or corner of the island shown in Fig. 2B. These data indicate a series of peaks, whose relative intensity varies with tip position. Spatial maps of dI/dV reveal standing wave patterns for the confined electrons (Figs. 2C-F). The energy levels of an electron in a two dimensional square box with infinitely high walls are given by:

$$E(n_x, n_y) = \frac{\hbar^2 \pi^2}{2m^*}\left(\frac{n_x^2 + n_y^2}{A}\right) + E_0 . \qquad \text{(Eq. 1)}$$

Here E_0 is the state energy for an infinite size box, n_x and n_y denote the energy level, m^* is the effective mass and A is the area of the box. The probability densities of eigenstates $|\psi_n|^2$ can be calculated analytically (insets in Figs. 2C-F), and are in good qualitative agreement with the experimental images. The effective mass for the 2 eV Cu_2N state, $m^* \approx 0.7\ m_e$, can be calculated from the spacing between levels (e.g. the (1,1) and (1,3 / 3,1) levels in Figs. 2C,E). For comparison, we calculated m^* of the corresponding band from our DFT band structure. Shown in red in Fig. 1C, the band is approximately parabolic near Γ, and can be fit with the equation: $E(k) = \frac{\hbar^2 k^2}{2m^*} + E_0$, using an effective mass of $m^* = 0.85\ m_e$ and E_0=2.1 eV, which is in reasonable agreement with experiment.

Figures 2(G-K) show corresponding data near the 4 eV state. In this case, it is difficult to resolve any distinct peaks in tunneling spectroscopy and only slight variation is observed with tip position. Spatial images of dI/dV show the ground state at ~3.9 V, but do not clearly show any higher excited states (Figs. 2J-K). To understand these differences, we consider the effective masses of the two bands. The reduced curvature of the 4 eV band in our DFT calculations (blue curve in Fig. 1C) indicates a larger effective mass $m^* = 2.4\ m_e$. From Eq. 1, the separation and spacing of confined levels from the band edge is inversely proportional to m^*, so that a weaker confinement effect is expected for bands with larger m^*. Given the intrinsic linewidth of these states (>0.1 eV), tunneling spectra and dI/dV images reflect the superposition of overlapping states, so that no single state can be resolved.

We studied the evolution of quantum confinement down to 0.5 nm^2 islands (corresponding to Cu_8N_4). In determining island areas from STM images (e.g. Fig. 3A), we consider broadening of island edges due to experimental (e.g. finite tip sharpness) and intrinsic (e.g. wave function leakage) sources (*4*). We defined the perimeter in atomic-resolution images as corresponding to one Cu layer beyond the boundary of N atoms (cf. Figure 3C). For islands in our data set where atomic resolution images were not obtained, we used a threshold technique to measure island areas (*28*). At low voltage (< 2.8 V), an island appears as a 0.18 nm depression relative to the bare Cu(100) surface. We chose a threshold of 30% of this depth for determining the island perimeter; this yielded an area consistent with the geometric area determined by counting atoms in atomic-resolution images (cf. contour in

Fig. 3C). We estimated the error in this method as the average variation in area for +- 5% changes in the threshold condition.

Figure 3B shows that the 2 eV state shifts toward higher energy as island area decreases, until it is no longer clearly observed in the smallest islands studied. The shift is summarized in Fig. 4 for a data set of 43 islands. Here the ground state energy was determined by fitting the lowest energy peak of spectra taken above the center of the islands. The scatter is likely due to shape variations, as many of the islands studied were not perfectly square. As expected from Eq. 1, the ground state energy is inversely proportional to island area. The linear trend suggests that the effective electron mass is independent of island area in this range; the slope gives $m^* \approx 0.98 \pm 0.08\ m_e$. The difference between this value and that obtained from the standing wave patterns on a single island ($0.7\ m_e$) likely indicates that our choice for defining the island perimeter underestimates the effective area of the island. As discussed previously (*29*), the wave functions of confined electrons may leak beyond the island boundaries. The leakage correction lowers m^*, and would be more important for the smaller islands in Figure 4, than for the large island in Figure 2. An effective mass $m^* = 0.85 \pm 0.1\ m_e$, in better agreement with the standing wave patterns and DFT calculations, is obtained using a 20% threshold criterion, roughly corresponding to an extra row of Cu atoms around the island perimeter.

We employed the 'constant current' mode to simultaneously monitor the evolution of both states with island area (Fig. 3D). Figure 4 shows that in contrast to the 2V peak, it is difficult to determine a systematic shift of the 4V peak. This likely indicates that the smaller shift expected for the heavier mass band is less than experimental uncertainties due to shape variation or environmental contributions, such as coupling to neighboring islands or point defects. Such environmental effects may explain why the rectangular island # 3 in Figure 3 exhibits a lower voltage peak (~3.7 V) than expected. Variation in the STM tip's sharpness or tip height (which differs by ~ 0.2 nm when probing the 2eV and 4eV states) (*10*) can also contribute systematic error, particularly for the smallest islands. For example, we found a ~0.1 V variation in peak position between sharp and blunt tips in studying several identical 0.5 nm^2 islands (i.e. data at $1/A$ = 1.9 nm^{-2} in Figure 4). This may indicate that the surrounding Cu contributes to the spatially averaged dI/dV probed by blunt tips over small islands.

Figures 3B,D show that both Cu_2N states can be clearly observed in islands down to ~1.5 nm^2. The 2 eV state is not observed in smaller islands, such as the 0.5 nm^2 island in Figure 3D, which only shows a weak peak associated with the 4 eV state. Although the

particle-in-a-box model provides good qualitative agreement for larger islands, it neglects aspects of the physical system which may be important for smaller islands. It is difficult for example, to measure the finite height barrier which confines electrons to the Cu_2N islands. A lower bound is 4 eV, as we still observe the confined ground state for the 4eV band. A reasonable upper bound is the Cu_2N work function, which we previously measured to be ~5.5 eV (*10*). In a finite height box with decreasing area, it is possible that the lower mass electrons in the ground state of the 2 eV band can no longer be confined while the higher mass electrons in the 4eV band can still be confined. However, extrapolation of the linear fit in Figure 4 to smaller islands suggests that electrons in the 2 eV band should still be confined, given our constraints on the barrier height.

We speculate that the disappearance of the 2 eV state in the smallest islands reflects a size-dependent coupling to available Cu states. At the Γ point, the projected band structure of the Cu(100) surface has an unoccupied surface state at ~1.8 eV and a gap from 1.8 eV to 7 eV (*30*). Electrons in the 2 eV state of Cu_2N may leak out from islands into the Cu surface state. The larger ratio of perimeter to area in smaller islands may increase the matrix elements coupling electrons in Cu_2N to the Cu surface state. This increased coupling could be responsible for the broadening with decreasing area illustrated in Fig. 3B. Similar broadening trends have been observed in other systems, and are typically attributed to lossy scattering at the island boundaries (*4*). In contrast, the 4 eV Cu_2N state lies well within the projected band gap of the Cu(100) surface, and is not near in energy to any Cu surface states. Leakage may still occur into bulk states, which can account for the observed broadening with decreasing area. However, the lack of available surface states may explain why the 4 eV state persists in the smallest islands studied (0.5 nm^2), comprising only 12 atoms.

This hypothesis is qualitatively consistent with our DFT calculations. Figure 1B shows calculated LDOS for 48- and 12-atom square islands, corresponding to islands #2 and #4 respectively in Figure 3A. Given the intrinsic noise in calculated LDOS from finite size systems, the quantum confined shifts of these states are difficult to resolve. However, we do find that the LDOS peak associated with the 2 eV state is reduced in the 48-atom island compared to the full monolayer, and is no longer visible in the 12-atom island. The LDOS associated with the 4 eV state also decreases, but a peak can still be observed in the smallest 12-atom islands. This trend is particularly clear in the *s*-state projected LDOS (bold curves in Fig. 1B). Furthermore, LDOS projected onto Cu sites within the Cu_2N islands (dashed curves) indicates that the 2 eV state has more Cu character than the 4 eV state, which may also facilitate the coupling to Cu surface states.

In summary, we demonstrate that a combination of scanning tunneling microscopy and density functional theory calculations is useful for studying the emergence of electronic states in nanoscale islands. Further extension of these methods will help in understanding the development of collective states in few-atom systems.

We thank K. Weaver for the particle-in-a-box calculations, and J. Nicklas, H. Park, A. Wadehra, and W. Windl for helpful discussions. We are grateful for support from the Center for Emergent Materials, an NSF MRSEC (DMR-0820414), NSF CAREER (DMR-0645451), and an allocation of computing time from the Ohio Supercomputer Center.

Figure Captions

Figure 1. Comparison of experimental and calculated electronic structure of Cu_2N. (A) Tunneling spectroscopy of a ~40 nm^2 island in *z*-ramp mode. The initial tip height was set at 5V, 1nA. Shown in red is the relative tip height as voltage is varied. (B) Calculated LDOS for monolayer (ML) coverage (black), and 48-atom (blue) and 12-atom islands (red). Total LDOS are projected onto N (thin solid lines) and Cu (dotted lines, x1/8) atomic sites. Thick solid lines are the N site *s*-state projection (x4 for 12,48-atom islands, x2 for ML). For clarity, LDOS for 48-atom and ML coverage are shifted by 0.5 and 1.0 units respectively. (C) Calculated band structure for a Cu_2N monolayer. Highlighted in red and blue are the two unoccupied Cu_2N bands. Open symbols show parabolic fits near Γ.

Figure 2. Quantum confinement in Cu_2N. (A,G) Tunneling spectroscopy with the tip positioned at the center and corner of the ~ 29 nm^2 island imaged in (B). The tip height was set at 3V, 1 nA in (A) and 5V, 0.5 nA in (G). The STM image in (B) was Laplace filtered to enhance contrast of the atomic lattice. A schematic showing Cu and N atomic positions is overlaid on part of the image. (0.5V, 1nA) (C-F) Spatial maps of dI/dV near 2V. Insets show probability density calculated using the simple particle-in-a-box model (H-K) Spatial maps of dI/dV near 4V.

Figure 3. Emergence of electronic states in nanoscale Cu_2N islands. (A) STM image showing four islands: (1) Irregular square, 6.4nm^2; (2) Square island ($Cu_{32}N_{16}$), 2.1 nm^2 ; (3) Rectangular island ($Cu_{24}N_{12}$), 1.6 nm^2; (4) Square island (Cu_8N_4), 0.5nm^2. (0.108V, 0.1nA) (B) Tunneling spectroscopy (constant height mode) near the 2 eV state. (3V, 1nA) (C) High resolution image of island #2, showing the lattice of Cu and N atoms. The contour represents the 30% threshold used to determine island area when atomic-resolution images were not available. (D) Tunneling spectroscopy (constant current mode) (0.25 nA).

Figure 4. Evolution of electronic states with island area. Shown are ground state peak positions for the 2 eV state (from constant height spectroscopy), and 4 eV state (from constant current spectroscopy). The solid line is a best fit using $m^* = 0.98\ m_e$.

References

1. M. F. Crommie, C. P. Lutz, D. M. Eigler, *Phys. Rev. B* **48**, 2851 (1993).
2. N. Nilius, T. M. Wallis, W. Ho, *Science* **297**, 1853 (2002).
3. J. Lagoute, X. Liu, S. Folsch, *Phys. Rev. Lett.* **95**, 4 (2005).
4. J. T. Li, W. D. Schneider, R. Berndt, S. Crampin, *Phys. Rev. Lett.* **80**, 3332 (1998).
5. N. Nilius, N. Ernst, H. J. Freund, *Phys. Rev. Lett.* **84**, 3994 (2000).
6. L. L. A. Adams, B. W. Lang, A. M. Goldman, *Phys. Rev. Lett.* **95**, 146804 (2005).
7. A. J. Heinrich, J. A. Gupta, C. P. Lutz, D. M. Eigler, *Science* **306**, 466 (2004).
8. F. E. Olsson, M. Persson, J. Repp, G. Meyer, *Phys. Rev. B* **71**, 075419 (2005).
9. S. Schintke, W. D. Schneider, *J. Phys. Condens. Matter* **16**, R49 (2004).
10. C. D. Ruggiero, T. Choi, J. A. Gupta, *Appl. Phys. Lett.* **91**, 253106 (2007).
11. F. M. Leibsle, S. S. Dhesi, S. D. Barrett, A. W. Robinson, *Surf. Sci.* **317**, 309 (1994).
12. T. Choi, C. D. Ruggiero, J. A. Gupta, *Journal of Vacuum Science & Technology B* **27**, 887 (2009).
13. J. Tersoff, D. R. Hamann, *Phys. Rev. B* **31**, 805 (1985).
14. R. Wiesendanger, *Scanning probe microscopy and spectroscopy : methods and applications*. (Cambridge University Press, Cambridge, 1994).
15. P. E. Blochl, *Phys. Rev. B* **50**, 17953 (1994).
16. G. Kresse, D. Joubert, *Phys. Rev. B* **59**, 1758 (1999).
17. J. P. Perdew, K. Burke, M. Ernzerhof, *Phys. Rev. Lett.* **77**, 3865 (1996).
18. G. Kresse, J. Hafner, *Phys. Rev. B* **47**, 558 (1993).
19. G. Kresse, J. Furthmuller, *Phys. Rev. B* **54**, 11169 (1996).
20. T. Lederer *et al.*, *Phys. Rev. B* **48**, 11277 (1993).
21. See EPAPS Document No. for raw LDOS calculations.
22. T. Michalke, R. Matzdorf, J. Braun, A. Postnikov, *Phys. Rev. B* **77**, 165425 (2008).
23. C. Baldacchini *et al.*, *Phys. Rev. B* **68**, 195109 (2003).
24. C. J. Chen, *Phys. Rev. Lett.* **65**, 448 (1990).
25. J. M. Blanco *et al.*, *Phys. Rev. B* **70**, 085405 (2004).
26. H. Jensen, J. Kroger, R. Berndt, S. Crampin, *Phys. Rev. B* **71**, 155417 (2005).
27. T. Michalke, Ph.D. Thesis, Univ. Wurzburg (2004).
28. I. Horcas *et al.*, *Rev. Sci. Instrum.* **78**, 013705 (2007).
29. L. Jensen, L. L. Zhao, G. C. Schatz, *J Phys Chem C* **111**, 4756 (2007).
30. P. Cortona, C. Sapet, *Int. J. Quantum Chem* **99**, 713 (2004).

Ruggiero et al., Figure 1

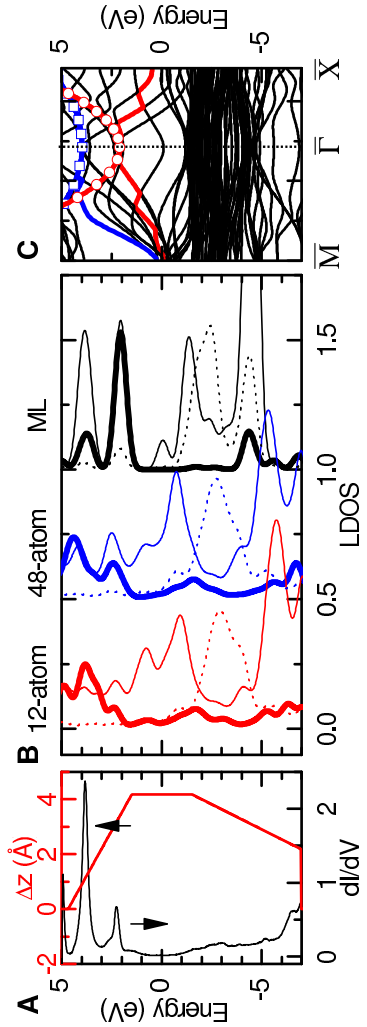

Figure 1 LS12698 03MAY2011

Ruggiero et al., Figure 2

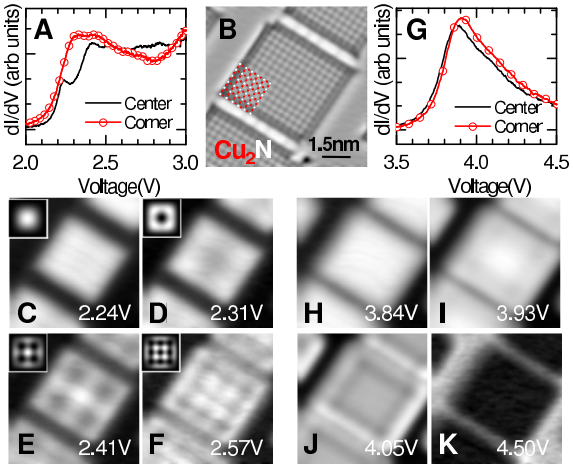

Figure 2 LS12698 03MAY2011

Ruggiero et al., Figure 3

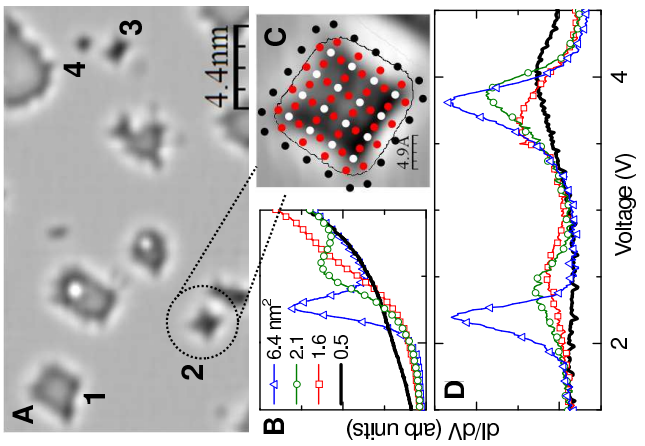

Figure 3 LS12698 03MAY2011

Ruggiero et al., Figure 4

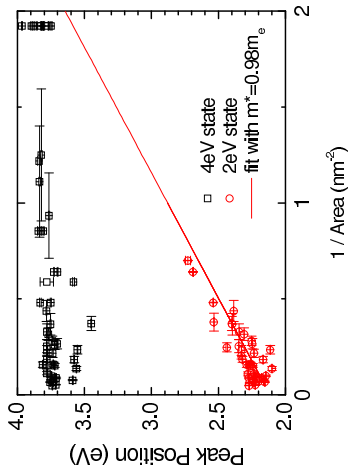

Figure 4 LS12698 03MAY2011